Nuclear matter and neutron star properties calculated with a separable monopole interaction

J. Rikovska Stone,[1,2] P. D. Stevenson,[1,3] J. C. Miller,[4,5] and M. R. Strayer[6]
[1]*Clarendon Laboratory, Department of Physics, University of Oxford, Oxford OX1 3PU, United Kingdom*
[2]*Department of Chemistry and Biochemistry, University of Maryland, College Park, Maryland 20742*
[3]*Department of Physics, University of Surrey, Guildford GU2 7XH, United Kingdom*
[4]*SISSA, via Beirut 2–4, I-34014 Trieste, Italy*
[5]*Nuclear & Astrophysics Laboratory, University of Oxford, Keble Road, Oxford OX1 3RH, United Kingdom*
[6]*Physics Division, Oak Ridge National Laboratory, Oak Ridge, Tennessee 37831-6373*
(Received 5 December 2001; published 3 June 2002)

This paper presents a further application of a new model for the effective two-body nucleon-nucleon interaction using a density-dependent separable monopole (SMO) interaction. This model has recently been successfully used for calculating the ground-state properties of spherical, doubly closed-shell nuclei from ^{16}O to ^{208}Pb and is used here to calculate properties of infinite symmetric nuclear matter and the beta-stable $n+p+e+\mu$ matter of relevance for neutron stars. An equation of state (EOS) is constructed for this and is joined smoothly onto the Baym, Pethick, and Sutherland EOS for baryon number densities below $n=0.1\ \mathrm{fm}^{-3}$ and onto the widely used Bethe-Johnson EOS at $n=0.5\ \mathrm{fm}^{-3}$. Nonrotating, zero-temperature neutron-star models have been calculated for this composite EOS and the results obtained are compared with those for models calculated with the Skyrme effective interaction and with realistic nucleon-nucleon potentials. The SMO interaction is shown to give excellent global agreement with a wide range of expected properties of infinite nuclear matter and of neutron stars.

DOI: 10.1103/PhysRevC.65.064312 PACS number(s): 21.65.+f, 26.60.+c, 21.30.Fe, 21.60.Jz

I. INTRODUCTION

The goal of nuclear structure theory is to describe the properties of observed nuclei given some model of the nuclear interaction as input. The difficulties in performing full-scale calculations, such as finding exact solutions of the many-body Schrödinger equation for finite nuclei, have led to *infinite nuclear matter* calculations becoming a standard approach for examining the properties of nuclear potentials. Both symmetric infinite nuclear matter (with equal numbers of protons and neutrons and with Coulomb effects being neglected) and also asymmetric nuclear matter [characterized by an asymmetry parameter $I=(N-Z)/A$] are of importance. Extrapolation of the density dependence of nuclear interactions to the subnuclear and supernuclear density regions of relevance for neutron stars introduces another perspective for investigations of matter under extreme conditions, which has direct relevance for studies of nuclei at the limits of stability with large values of isospin.

Since the 1970s two principal types of effective density-dependent two-body nuclear potentials have mainly been used in nonrelativistic Hartree-Fock mean-field calculations for finite nuclei: zero range Skyrme interactions [1] and finite range Gogny interactions [2]. There are many known parametrizations of these potentials that reproduce basic experimental data for finite nuclei and the observable properties of infinite symmetric matter with more or less comparable success. A more stringent test of the validity of these interactions, especially their isospin-dependent part, can come from investigating asymmetric infinite and semi-infinite nuclear matter. A modified Skyrme interaction, emphasizing the isovector term in the potential, has been used to model thermodynamical properties of hot, dense nuclear matter [3]; Onsi, Przysiezniak, and Pearson [4] used several Skyrme interactions in their investigation of the equation of state (EOS) of homogeneous nuclear matter under conditions appropriate for a collapsing star, employing the Extended-Thomas-Fermi-Strutinsky-Integral (ETFSI) approximation to the Hartree-Fock method, and a modified SIII interaction was used by Pethick, Ravenhall, and Lorenz [5] for describing the matter of a neutron-star crust in beta equilibrium. An attempt to determine parameters of a Skyrme interaction describing nuclear matter from subnuclear to neutron-star densities was presented by Chabanat *et al.* [6].

Cold, nonrotating neutron stars offer an extraordinary laboratory for investigations of nuclear matter. Developing an equation of state (i.e., the functional dependence of the pressure P on the mass density ρ) for the whole range of densities relevant for neutron stars by means of a single unified calculation is beyond the scope of all current studies and so it is common practice to make a composite EOS, consisting of different parts describing physical processes in particular, density regions, matched smoothly at transition points between the regions. It is standard to use the EOS of Baym, Pethick, and Sutherland [7] for the density range below $\sim 10^{14}$ g/cm^3. The region up to two to three times the nuclear saturation density ($\sim 2.7\times 10^{14}$ g/cm^3—the density corresponding to the minimum energy per nucleon in symmetric nuclear matter) is well modeled as free nucleon + lepton matter and can be used for testing nonrelativistic mean-field models with phenomenological interactions (e.g., [6]) as well as realistic nuclear interactions [8–11]. For higher densities, many attempts to construct an EOS for the region above the threshold for the creation of hyperons (and, possibly, heavy mesons) can be found in the literature based both on nonrelativistic approaches (e.g., [12–14]) and relativistic mean-field (RMF) ones [15–17]. Speculative models, considering the presence of deconfined quarks in the center

 ©2002 The American Physical Society

TABLE I. Parameters of the separable monopole interaction.

	W_a (MeV fm^3)	α_a	β_a	a_a	b_a
SMO1	−1543.8	2.0	1.0	−0.4295	−0.4448
SMO2	−1545.0	2.0	1.0	0.5000	−0.2600
	W_r (MeV fm$^{1-\alpha_r+2\beta_r}$)	α_r	β_r	a_r	b_r
SMO1	1778.0	2.2165	1.246	−1.4788	−0.3146
SMO2	1710.0	2.22400	1.240	−0.45	−0.1650
	c (MeV fm^5)	k (MeV fm^{10})			
SMO1	160.0	16.0			
SMO2	190.0	16.0			

of neutron stars, have been presented in a number of recent publications [10,18–21].

When an appropriate EOS has been constructed, nonrotating neutron-star models can be calculated by integrating the Tolman-Oppenheimer-Volkoff (TOV) equations. Important properties of the models, such as the mass-radius relation, the binding energy, the total number of baryons, the moment of inertia, and the maximum rotation speed can be calculated and compared with values coming from observations. Among the most important parameters are the mass of the maximum-mass model and the radius of a canonical 1.4 solar mass model (thought to be representative for many observed neutron stars). The properties of the maximum-mass models depend critically on the choice of the EOS at high densities and thus are not a sensitive test of the EOS at around the nuclear saturation density. However, the properties of lower mass models and the overall mutual consistency of the individual components in a composite EOS serve as important indicators of the validity of the treatment in the various density regions.

It is the aim of this paper to test the newly developed separable monopole (SMO) interaction [22] by using it to calculate a wide range of nuclear matter properties. After a brief description of the SMO approach in Sec. II, in Sec. III we calculate properties of infinite symmetric nuclear matter ($I=0$) and pure neutron matter ($I=1$) as well as of asymmetric $n+p+e+\mu$ matter in beta equilibrium. In Sec. IV, an SMO EOS is constructed and used for calculating nonrotating neutron-star models. Section V is the Conclusion.

II. THE SEPARABLE MONOPOLE INTERACTION

This two-body interaction, used previously for finite nuclei [22], consists of two main parts (attractive and repulsive) that have the same mathematical form for the density and isospin dependence and differ only in the values of adjustable parameters. Having attractive and repulsive terms with different ranges is a common feature of density-dependent effective interactions and it is these terms that are responsible for most of the binding energy in finite nuclei and for the volume energy in nuclear matter.

Each term in the expression for the interaction is separable in the space coordinates (and in isospin where applicable). This is the essential new property of this effective nucleon-nucleon interaction that makes it suitable for building a perturbation series in powers of the strength of the SMO interaction in order to include correlations in finite nuclei, beyond the mean field, with convergent results. We will see that the separability also has an important consequence for calculating perturbations in nuclear matter. The interaction is written in coordinate space as

$$\begin{aligned} V(\vec{r}_1,\vec{r}_2) = {} & W_a f_a n^{\beta_a}(\vec{r}_1) n^{\beta_a}(\vec{r}_2) \\ & \times [1 + a_a(t_1^+ t_2^- + t_1^- t_2^+) + 4 b_a t_{1z} t_{2z}] \\ & + W_r f_r n^{\beta_r}(\vec{r}_1) n^{\beta_r}(\vec{r}_2) [1 + a_r(t_1^+ t_2^- + t_1^- t_2^+) \\ & + 4 b_r t_{1z} t_{2z}] \\ & + k \nabla_1^2 n(\vec{r}_1) \nabla_2^2 n(\vec{r}_2), \end{aligned} \tag{1}$$

where the function f_ξ, which ensures the correct mass number dependence of the potential [22], is defined as

$$f_\xi = \left[\int d^3\vec{r}\, n^{\alpha_\xi}(\vec{r}) \right]^{-1} \tag{2}$$

for subscripts $\xi = a$ and $\xi = r$; t^+, t^- and t_z are isospin raising and lowering operators and the z-axis projection operator. The one-body spin-orbit potential is given by

$$V_{s-o}(r) = c \frac{1}{r} \frac{\partial n}{\partial r} \vec{l} \cdot \vec{s} \tag{3}$$

and the Coulomb potential has the standard form [22]. W_a, α_a, β_a, a_a, b_a, W_r, α_r, β_r, a_r, b_r, k, and c are parameters whose values have been fixed by fitting to the ground state properties of 14 doubly closed-shell (subshell) finite nuclei [22]. The parameter set, labeled as SMO1, is given in Table I. In nuclear matter, for which the density is taken to be constant, the derivative and the spin-orbit terms are identically zero.

In line with the notation normally used for studies of nuclear matter in astrophysics, we use $n = n_p + n_n$ for baryon number densities in fm^{-3} rather than $\rho = \rho_p + \rho_n$, which is used in this paper to denote mass densities in g/cm^3.

III. INFINITE SYMMETRIC AND ASYMMETRIC NUCLEAR MATTER

A. Properties and observables

In this section we detail the properties that any model needs to predict for comparing with quantities extracted from observable data.

The *binding energy per particle* $\mathcal{E}$ of infinite nuclear matter can be written as a function of the baryon number density n and the asymmetry parameter $I=(N-Z)/A$. In this way, the same expression can be used for symmetric and asymmetric matter. For the SMO interaction, we get

$$\mathcal{E}(n,I)=c_p\frac{1}{2^{5/3}}(1-I)^{5/3}n^{2/3}+c_n\frac{1}{2^{5/3}}(1+I)^{5/3}n^{2/3}+\frac{1}{2}W_a n^{2\beta_a-\alpha_a+1}+\frac{1}{2}W_r n^{2\beta_r-\alpha_r+1}+\frac{1}{2}W_a b_a n^{2\beta_a-\alpha_a+1}I^2+\frac{1}{2}W_r b_r n^{2\beta_r-\alpha_r+1}I^2 \tag{4}$$

(for a full derivation and explanation of the notation see Appendix A). The value of $\mathcal{E}$ at saturation (i.e., the minimum value) is usually taken to be the coefficient of the volume term a_v in the liquid-drop model, obtained by fitting with the binding energies of a large number of nuclei. This procedure gives $\mathcal{E}_0=-(16.0\pm0.2)$ MeV [6]. However, a somewhat lower value [$\mathcal{E}_0=-(15.6\pm0.2)$ MeV] has been quoted recently by Heiselberg and Hjorth-Jensen [11]. The density n_0 of symmetric nuclear matter at saturation is expected to be $n_0=0.16\pm0.005$ fm^{-3} [6] based on calculating the charge distribution in heavy nuclei. A more conservative value of 0.17 ± 0.02 fm^{-3} is given in Ref. [23] where the error bar includes uncertainties in the neutron density distribution and a correction for possible density inhomogeneity in the nuclear interior. The value quoted in Ref. [11] (0.16 ± 0.02 fm^{-3}) is of the same precision as that in Ref. [23].

The *pressure* P in nuclear matter is defined as [11]

$$P(n)=n^2\frac{\partial\mathcal{E}}{\partial n}=n\frac{\partial\epsilon}{\partial n}-\epsilon, \tag{5}$$

where $\epsilon=n(\mathcal{E}+mc^2)$ is the total energy density and m is the nucleon mass.

Another property of interest in discussing nuclear matter and equations of state is the *incompressibility modulus* K of symmetric nuclear matter. This is defined as a function of n [6]:

$$K(n)=9n^2\frac{\partial^2\mathcal{E}}{\partial n^2}+18\frac{P(n)}{n}. \tag{6}$$

The value of K_∞, at saturation ($P=0$), represents an important constraint on models of nuclear matter. However K is a derived quantity and its ''best'' value is model dependent. Nix and Moller estimate $K_\infty\simeq240$ MeV [24], while Hartree-Fock+random phase approximation (RPA) calculations of the giant isoscalar monopole resonance (the breathing mode) [25] imply $K_\infty=(210\pm20)$ MeV both with the use of Skyrme interactions [26] and with the Gogny potential [27]. The generalized Skyrme interactions [28], fitted both to finite nuclei and the breathing mode energies, give the best results for $K_\infty=(215\pm15)$ MeV.

For the SMO interaction, the generalized incompressibility modulus is given as

$$K(n)=-2a_k n^{2/3}+\frac{9}{2}W_a(2\beta_a-\alpha_a+1)\times(2\beta_a-\alpha_a)n^{2\beta_a-\alpha_a+1}+\frac{9}{2}W_r(2\beta_r-\alpha_r+1)\times(2\beta_r-\alpha_r)n^{2\beta_r-\alpha_r+1}+18\frac{P(n)}{n}. \tag{7}$$

In the nonrelativistic approximation, the *speed of ordinary sound* in the nuclear medium is related to the incompressibility modulus K by [11]

$$\frac{v_s}{c}=\frac{dP(n)}{d\epsilon}=\sqrt{\frac{K(n)}{9\left(mc^2+\mathcal{E}+\frac{P(n)}{n}\right)}}. \tag{8}$$

It is desirable to follow the density dependence of the speed of sound as it may exceed the velocity of light at higher densities in nonrelativistic models [11] and this unrealistic feature must be taken care of. The *adiabatic index* Γ can also be calculated from the EOS [11]:

$$\Gamma=\frac{n}{P}\frac{\partial P}{\partial n}. \tag{9}$$

Another important variable in any discussion of asymmetric nuclear matter is the *symmetry energy*, defined as the difference in energy between symmetric and pure neutron matter. This is directly related to the *asymmetry coefficient* a_s in the well-known Bethe-Weizsäcker semiempirical mass formula [29]. For the SMO interaction, a_s is expressed as

$$a_s=\frac{5}{36}c_p n^{2/3}+\frac{5}{36}c_n n^{2/3}+\frac{1}{2}W_a b_a n^{2\beta_a-\alpha_a+1}+\frac{1}{2}W_r b_r n^{2\beta_r-\alpha_r+1}. \tag{10}$$

The value of a_s ($=32.5\pm0.5$ MeV [30]) is found by fitting to a large set of experimental data in the finite-range-droplet model. More recently, Tondeur *et al.* [31] have advocated a lower value of 28 MeV from their fit of nuclear ground state binding energies in a mean-field model with a Skyrme interaction. Heiselberg and Hjorth-Jensen [11] put typical values of a_s in the region of 27–38 MeV, as obtained with nonrelativistic Hartree-Fock theories, and Li, Ko, and Ren [32] quote a 35–42 MeV range of predictions for a_s coming from RMF models.

In addition, one may consider pure neutron matter. Although no observables as such are known, due to the fact that neutron matter is not bound by nuclear forces, this very fact is an important constraint, i.e., *neutron matter should not be predicted to be bound* by the model. The energy per particle of pure neutron matter is given by Eq. (4) with $I=1$ and $n=n_n$:

$$\mathcal{E}(n,1)=c_n 2^{2/3} n^{2/3}+\frac{1}{2}(1+b_a)W_a n^{2\beta_a-\alpha_a+1}$$

$$+\frac{1}{2}(1+b_r)W_r n^{2\beta_r-\alpha_r+1}. \quad (11)$$

B. Perturbation calculations

The SMO interaction has been shown to give a converging perturbation series describing nucleon correlations beyond the mean field in finite nuclei [22]. In the case of infinite nuclear matter with constant density in space, the Hartree-Fock solution consists of a Slater determinant of plane wave states (see Appendix A). For a separable, density-dependent interaction, the perturbative corrections to the ground state binding energy are given by a series of terms, each containing a product of a number of interaction matrix elements commensurate with the order of the perturbation [22]. In every case, however, one of these matrix elements contains only particle states in the bra ($\langle p_1 p_2|$) and hole states in the ket ($|h_1 h_2\rangle$). This matrix element has the form

$$\langle p_1 p_2|g(n(r_1))g(n(r_2))|h_1 h_2\rangle = g^2\langle p_1|h_1\rangle\langle p_2|h_2\rangle, \quad (12)$$

where $g(n(r_i))$ stands here symbolically for the density-dependent function in the interaction [see Eq. (1) and Ref. [22]] and is a finite constant in space in the nuclear matter due to the constant density. Because the particle and hole states are always orthogonal, the overlap matrix elements calculated in the above expression are zero. Thus perturbations to the wave functions, representing contributions from correlations in nuclear matter, are zero to all orders for a density-dependent separable interaction.

This result is a direct consequence of the separability of the interaction, which dictates the particular form of the terms in the perturbation series. Physically, SMO models nuclear matter as a system of nucleons interacting only through the mean field with no residual nucleon-nucleon interaction beyond it. We show in the following sections that this model is fully adequate for giving a correct detailed description of nuclear matter properties in the relevant range of baryon number densities.

Other (nonseparable) effective nucleon-nucleon interactions (e.g., the Skyrme potentials) also describe nuclear matter properties well in mean-field models [6]. One usually considers that short-range correlations are already included in the Skyrme mean field. Identification and treatment of those correlations beyond the mean field is difficult; these potentials are divergent in order-by-order perturbation theory and only a treatable subset of perturbation terms (e.g., the RPA) can be studied.

TABLE II. Properties of infinite nuclear matter at equilibrium for the SMO1 and SMO2 interactions. Results for the SLy230a and MSk6 Skyrme interactions [6,31] are included for comparison. The observables listed are the equilibrium density, n_0 (fm^{-3}), the Fermi momentum k_F (fm^{-1}), the mean distance between two nucleons in the fluid, $r_0=(9\pi)^{1/3}/2k_F$ (fm), the energy per particle of symmetric nuclear matter at the saturation density n_0, $\mathcal{E}_0$ (MeV), the incompressibility modulus of symmetric infinite nuclear matter at saturation, K_∞ (MeV), the effective mass m_∞^*/m, and the asymmetry coefficient a_s (MeV). For empirical values see text.

Interaction	SMO1	SMO2	SLy230a	MSk6
n_0	0.155	0.170	0.160	0.158
k_F	1.320	1.360	1.333	1.326
r_0	1.154	1.120	1.143	1.148
$\mathcal{E}_0$	−15.55	16.0	−16.0	−15.8
K_∞	218	221	230	231
m_∞^*/m	1.0	1.0	0.7	1.05
a_s	37.7	31.7	32.0	28

This scenario is fundamentally different from models with a realistic nucleon-nucleon interaction, where the empirical saturation properties of nuclear matter cannot be reproduced assuming this interaction between structureless nucleons alone (see, e.g., Ref. [10] and references therein). Correlations between nucleons should ideally be taken into account in the form of a perturbation expansion in powers of the strength of the nucleon-nucleon interaction. However, this series diverges because the interaction is too strong, and the expansion has to be rearranged by using partial summations or similar techniques and this affects the accuracy of the calculation.

C. Results and discussion

1. The SMO parametrizations

In Ref. [22] we gave an extensive discussion of a parametrization of the separable monopole interaction, which we refer to in this paper as SMO1 (see Table I). This gives excellent agreement with observed one-body nuclear ground state properties (charge radii and density distributions) and gives ground state binding energies of doubly closed-shell nuclei from ^{16}O to ^{208}Pb, which are in fair agreement with experiment—the differences seen could probably be removed by extending the present monopole potential to include terms with higher multipolarity (extending the perturbation theory to include higher order correlations) and making a more realistic description of the surface and spin-orbit terms. SMO1 also gives good agreement with the observables of symmetric infinite nuclear matter with the exception of a rather high value for the asymmetry coefficient a_s of 37.7 MeV (see Table II) and a rather high radius for a canonical $1.4M_\odot$ neutron star of ~12.10 km (see Table IV). The asymmetry energy is directly related to the choice of the parameters b_a and b_r of the isospin-dependent part of the interaction and thus serves as an important constraint on possible values of these two parameters, but the canonical neutron-star radius is dependent also on other factors. To

TABLE III. Parameters of maximum-mass neutron-star models: n_c and ρ_c are the central number density and mass density, R is the radius, M is the mass, A is the total baryon number, $E_{\rm bind}$ is the binding energy, and $z_{\rm surf}$ is the surface gravitational redshift (see Ref. [6]). All of the EOS's were matched to the BPS EOS at low densities (see text). Results in the first two columns are for the full composite SMO EOS, including the Bethe-Johnson EOS at high densities. Results for a realistic potential from Akmal, Pandharipande, and Ravenhall [10] and a Skyrme interaction Sly230a [6] are included for comparison.

Interaction	SMO1 +BPS+BJ	SMO2 +BPS+BJ	SMO1 +BPS	SMO2 +BPS	A18+ δv +UIX*	SLy230a
n_c (fm^{-3})	1.29	1.31	1.26	1.31	1.14	1.14
ρ_c (10^{14} g cm^{-3})	29.98	30.58	29.68	30.73	27.28	27.00
R (km)	10.01	9.87	10.03	9.81	10.0	10.22
M ($M_\odot$)	1.86	1.85	1.92	1.88	2.20	2.09
A ($/10^{57}$)	2.56	2.56	2.64	2.60	3.21	2.96
$E_{\rm bind}$ (10^{53} erg)	5.01	5.08	5.08	5.24	8.59	6.80
$z_{\rm surf}$	0.487	0.497	0.503	0.516	0.689	0.589

improve the results, we performed a simultaneous fit to the asymmetry coefficient a_s and to the following quantities for symmetric infinite nuclear matter: the saturation density n_0, the energy per particle $\mathcal{E}$, and the incompressibility modulus K_∞. We also included in the fit the density dependencies of the energy per particle of symmetric and pure neutron matter and the electron chemical potential μ_e of beta-equilibrium nucleon+lepton matter, as calculated using the A18+ δv +UIX* realistic potential [10]. The new parametrization, SMO2, gives $a_s=30.9$ MeV and the radius of a $1.4M_\odot$ neutron star as 11.67 km, both closer to the expected values. SMO2 was then used without change for finite nuclei. A fit to the one- and two-body properties of doubly closed shell nuclei of comparable quality to that obtained for SMO1 was achieved by adjustment of the parameters that do not contribute to nuclear matter properties (a_a and a_r and the spin-orbit strength c). The values of the parameters for SMO2 and the results obtained with this for nuclear matter and neutron-star properties are shown in Tables I–IV.

2. Infinite nuclear matter

In Table II we show calculated values for the observables of infinite symmetric nuclear matter. Results for the Skyrme SLy230a interaction [6] are given for comparison. The dependence of the energy per particle $\mathcal{E}$ [Appendix A, Eq. (A14)] on baryon number density for symmetric and pure neutron matter is shown in Fig. 1. The saturation density n_0 for symmetric nuclear matter occurs within the limits of the inferred empirical value for both SMO1 and SMO2 as can be seen from Table II. Also, pure neutron matter remains unbound over the whole region of densities shown in Fig. 1 (right panel) as required.

The characteristic properties of asymmetric nuclear matter vary as a function of the proton fraction y_p, defined as the ratio of the number of protons to the total number of baryons. (The parameter y_p is frequently used in the astrophysics literature and is related to the asymmetry parameter I, introduced earlier by $I=1-2y_p$). It is instructive to calculate the energy per particle $\mathcal{E}$, the incompressibility modulus K, and the speed of sound v_s as functions of a fixed (i.e., density-independent) proton fraction y_p, for nuclear matter consisting only of protons, neutrons, and electrons.

It is expected that any reasonable nuclear interaction should exhibit the following behavior [6,33].

(i) The saturation density n_0 should decrease with an increasing proportion of neutrons.

(ii) The incompressibility modulus K should increase with increasing isospin asymmetry and the value of K at saturation should decrease with increasing y_p.

(iii) The sound velocity v_s at any density should increase with an increasing proportion of neutrons.

The above features are demonstrated in Fig. 2 for the SMO2 interaction (the SMO1 gives very similar results). It is gratifying to observe that the separable interaction, which is

TABLE IV. The same as Table III, but for a "standard" $1.4M_\odot$ neutron star.

Interaction	SMO1 +BPS+BJ	SMO2 +BPS+BJ	SMO1 +BPS	SMO2 +BPS	A18+ δv +UIX*	SLy230a
n_c (fm^{-3})	0.57	0.59	0.54	0.59	0.55	0.51
ρ_c (10^{14} g cm^{-3})	10.49	10.92	10.19	10.97	9.93	9.26
R (km)	12.09	11.77	12.11	11.76	11.47	11.77
M ($M_\odot$)	1.40	1.40	1.41	1.41	1.40	1.39
A ($/10^{57}$)	1.83	1.85	1.84	1.86	1.86	1.84
$E_{\rm bind}$ (10^{53} erg)	2.29	2.54	2.28	2.55	2.74	2.55
$z_{\rm surf}$	0.233	0.243	0.234	0.244	0.250	0.240

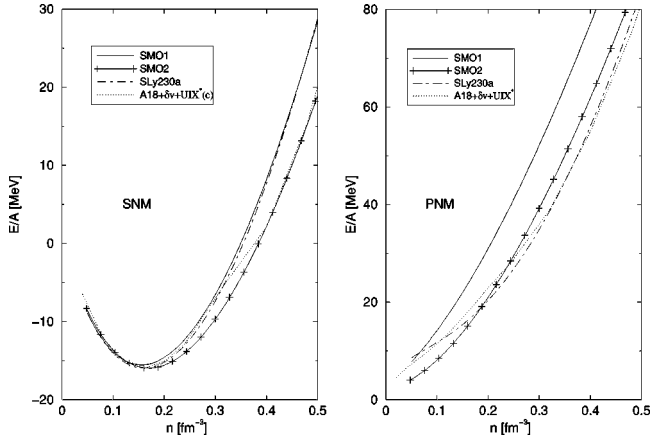

FIG. 1. The energy per particle for symmetric nuclear matter, SNM, (left panel) and pure neutron matter, PNM, (right panel) are plotted as functions of the baryon number density n for the SMO1 and SMO2 interactions. The same quantities for the Skyrme SLy230a interaction [6] and the A18+ δv + UIX* interaction [10] are included for comparison.

inherently very different from the realistic or Skyrme potentials, behaves in the expected way even for these detailed features. The velocity of sound is well below the velocity of light in the region of applicability of the present model (up to about twice the nuclear saturation density).

3. Beta-stable $n+p+e+\mu$ matter

The parameters of beta-stable nucleon+lepton matter (see Appendix B) have been calculated as a function of the baryon number density. For any model it is particularly important to predict the correct density dependence of the asymmetry coefficient a_s; this coefficient is directly related to the proton fraction y_p in beta-equilibrium matter and is thus relevant for the composition of the neutron-star matter. In Fig. 3 we show calculated values of a_s for the SMO1 and SMO2 interactions and compare them with values given by selected Skyrme interactions. Good agreement is found between the dependence of the asymmetry energy a_s and the proton fraction y_p on the particle density for SMO2 and some of the Skyrme interactions (SLy230a [6] and SkO [34]) and the behavior predicted by calculations [11] (see Fig. 4) made with a variety of realistic effective potentials. The proton fraction y_p rises steadily through the density region up to $n=1.0$ fm^{-3}, reaching about 15%. The asymmetry coefficient increases from ~20 to 80–100 MeV in the same density region.

A quite different behavior is exhibited by some Skyrme interactions (SkX [35] and MSk6 [31]); in particular, negative symmetry energies and a sharply decreasing number of protons at densities below two to three times the nuclear saturation density are predicted. Similar effects were observed by Onsi, Przysiezniak, and Pearson [4] for neutral nuclear matter ($n+p+e+\nu$), where the SkSC4 interaction predicted a rapid decrease of the proton fraction at densities ~0.2 fm^{-3}. The authors quote a comment by Lattimer that this result would imply a nonphysical collapse of neutron stars.

The disappearance of protons was also observed by Wiringa, Fiks, and Fabrocini [8] for the AV14+UVII, UV14 +UVII, and UV14+TNI potentials, although at densities higher than 1.5 fm^{-3} for the first two potentials. This effect was attributed to a particular feature of the potentials, namely, the greater short-range repulsion in isospin singlet nucleon pairs as compared with isospin triplet pairs. It was argued that at high densities, the short-range repulsion must dominate and thus pure neutron matter is favored. However, as discussed above, many current realistic potentials predict that the proton fraction y_p increases up to at least $n=1.0$ fm^{-3}, as illustrated in Fig. 4.

The presence of protons in nuclear matter at supernuclear densities is directly relevant for modeling the composition of neutron-star matter at densities higher than two to three times n_0. There are two main issues to be discussed in this context.

First, if protons are not present at densities of $(2-3)n_0$, neutron-star matter is then a on e component medium consisting only of interacting, homogeneous unpolarized neutrons. The EOS for pure neutron matter is seen as a first approximation for calculating parameters of neutron stars

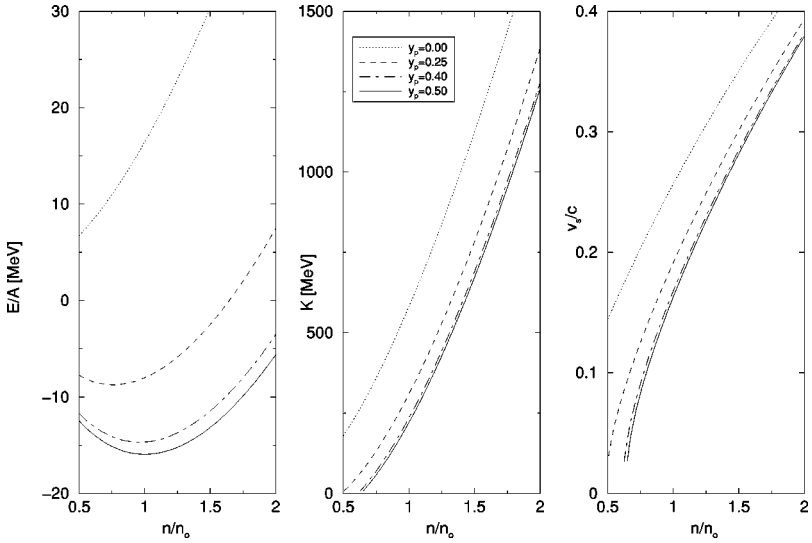

FIG. 2. The energy per particle E/A (left panel), the incompressibility coefficient K (middle panel), and the velocity of sound v_s (right panel) for various fixed values of the proton fraction y_p are plotted as functions of the baryon number density for the SMO2 interaction. The saturation densities n_0 (and incompressibility K) for $y_p=0.25$ and 0.40 are 0.129 (137) and 0.163 (207) fm^{-3} (MeV), respectively.

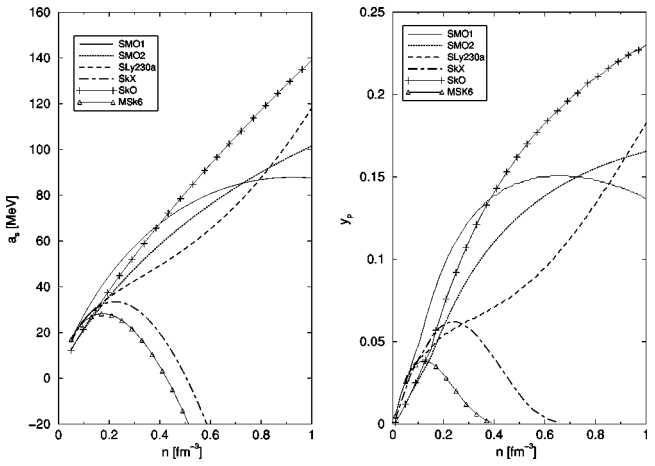

FIG. 3. The asymmetry energy coefficient a_s and the proton fraction y_p for beta-stable $n+p+\mu+e$ matter are plotted as functions of the baryon number density n. Results for some selected Skyrme interactions are included for comparison. See text for more details.

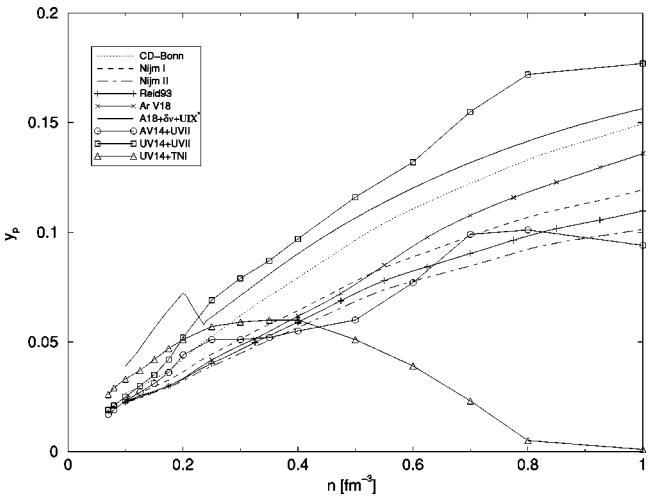

FIG. 4. The proton fraction y_p for beta stable nucleon+lepton matter, as calculated using various realistic potentials, is plotted as a function of the baryon number density n. The data have been taken from Refs. [8,10,11]. These curves should be compared with the SMO1 and SMO2 results shown in Fig. 3.

(see Refs. [36] for a review of early works, [37,38] and references therein). The usual consequence of using a pure neutron matter EOS is the prediction of a rather high maximum mass because of lacking the ''controlling'' effect on the pressure that some other constituents (e.g., hyperons) may have [39]. However, it has been pointed out by Pandharipande [40] that under certain circumstances (e.g., if the average heavy baryon-baryon interaction is less attractive than the *n-n* interaction) the pure neutron equation of state is a fairly good approximation to that of hyperonic matter.

The present consensus favors models of neutron-star matter including new hadronic degrees of freedom in addition to neutrons and protons. These can come from the formation of hyperons (strange baryons), meson condensation, or formation of a deconfined quark phase [39]. In cold, beta-stable, and neutrinoless neutron-star matter, hyperons should appear at densities as low as $2n_0$ and form a considerable fraction of the total baryon population by $n=3n_0$ [39]. All models including hyperons estimate the hyperon-hyperon and hyperon-nucleon interactions using growing experimental data for hypernuclei with $y_p \sim 10\%$ at $n=1.2$ fm^{-3}. All of these results are dependent on models of the hyperon-hyperon interaction (see, e.g., [41]), which are not yet very well constrained despite the increasing amount of experimental data on hypernuclei [42] and hyperon-nucleon scattering [43]. The basic effect of having hyperons in matter at high density is a softening of the equation of state because of the increase in the number of degrees of freedom, which relieves some of the pressure of the nucleons [39]. This in turn implies a lower maximum mass for neutron stars, as we will discuss in the following section.

The second issue for which the proton fraction as a function of matter density is important regards neutron-star cooling either just after their birth in supernovae or after heating in an accretion episode. A detailed discussion of this complex problem is beyond the scope of the present paper (for a review see, e.g., [44,45]. Although many models of cooling exist, (mainly involving emission of neutrinos from the stellar core) observational evidence does not yet conclusively point to any particular one of them. We only comment here that if, for example, the rapid neutrino cooling connected with the direct Urca process (involving weak interactions between nucleons) were demonstrated to be taking place in neutron stars, this would provide a powerful constraint on nuclear potentials. (There are indeed some recent indications that this may have been seen [46].) The minimum proton concentrations for the reactions in the direct Urca process to proceed are $\sim 11\%$ in $n+p+e$ beta-stable matter below the μ^- threshold and $\sim 15\%$ in $n+p+e+\mu$ above it [44].

An interesting suggestion has recently been made for obtaining experimental data about the proton concentration in neutron-star matter from neutron-rich heavy-ion collisions at intermediate energies, and the first data for this has already been published [32]. Another possible nuclear physics approach can involve studies of the density distribution of neutron-rich nuclei [47].

Figure 5 shows the electron chemical potential in beta-stable $n+p+e+\mu$ matter as a function of the baryon number density, as calculated with the SMO models, in comparison with results for the SLy230a Skyrme interaction [6] and the A18$+\delta v+$UIX* realistic potential [10]. It can be seen that the SMO results agree well with those obtained with the other potentials. All of the models also predict the threshold density for μ^- production to be in a narrow range around 0.17 fm^{-3} with the exception of the SMO1 model, where the threshold is slightly lower.

The electron and neutron chemical potentials are two independent quantities determining the chemical equilibrium in multicomponent matter (e.g., [39,48]). The density dependence of the neutron and proton chemical potentials is related to the choice of the model for the nucleon-nucleon interaction. Figure 6 shows the behavior of μ_n, μ_p, and μ_e and the corresponding relative particle fractions in beta-stable $n+p+e+\mu$ matter for three different effective inter-

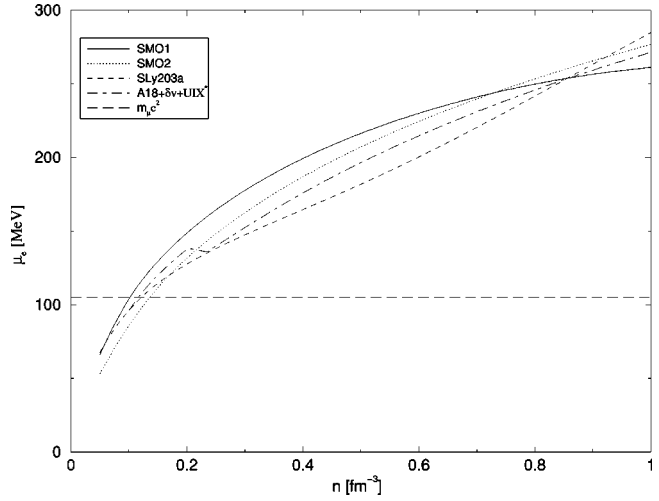

FIG. 5. The electron chemical potential μ_e for beta-stable matter as calculated with the SMO, SLy230a Skyrme [6], and A18 $+\delta v+$UIX* [10] interactions.

actions. We see that despite the differences in the density dependence of μ_n and μ_p for the SMO2 and SLy230a interactions, the concentrations of particles in the matter are rather similar and comparable, for example, to the composition calculated with the A18$+\delta v+$UIX* realistic potential [10]. This can be understood because particle fractions are dependent only on the *difference* $\mu_n-\mu_p=\mu_e=\mu_\mu$. However if μ_p increases above μ_n, the electron chemical potential becomes negative, thus preventing the production of leptons, and the matter undergoes an unphysical transition to a pure neutron system (see Fig. 6, for the MSk6 interaction).

The electron and neutron chemical potentials control the threshold densities for the production of heavy mesons and baryons in matter in chemical equilibrium. However, as the interactions of these particles amongst themselves and with the nucleons are poorly known, these thresholds are uncertain. However, some interesting results can be obtained even without an exact calculation of the hyperon chemical potential. The minimum value of the potential for a noninteracting Σ^- hyperon (which, in all models of hyperonic matter, appears at the lowest density in $n+p+e+\mu$ matter) is equal to its rest mass. The threshold depends on the sum of μ_n and μ_e,

$$\mu_{\Sigma^-}=\mu_n+\mu_e=m_{\Sigma^-}. \tag{13}$$

For the models shown in Fig. 6 and taking $m_{\Sigma^-}=1197$ MeV, we get threshold densities of 0.30 and 0.34 fm^{-3} for SMO2 and SLy230a, respectively. These estimates assume a noninteracting Σ^- hyperon, although some recent experimental work suggests a strong isoscalar repulsion in the interaction of Σ hyperons with bulk nucleons [49]. In the MSk6 model, only hyperons whose decay involves protons can appear. As can be seen in Fig. 6, μ_n never rises above 1000 MeV in the region of densities where the $n+p+e+\mu$ matter model is valid and so Σ^- hyperons are not produced.

The adiabatic index Γ and the velocity of sound in units of c, as calculated for the SMO interactions, are shown in Fig. 7. Results for the SLy230a and MSk6 Skyrme interactions have been included for comparison. The small jump in Γ at densities $\sim$0.17 fm^{-3} for the SMO models corresponds to the threshold of μ^- production. When no new particles are created, Γ exhibits a steady trend as a function of density, as expected. These results are very similar to those obtained with the SLy230a interaction except that the effect of the onset of muon production is not visible there. The dot-dashed curve in the top part of the figure represents the parts of the $\Gamma(n_b)$ curve for the MSk6 model which lie in the expected range of values between 1–3 (for a discussion of expected limiting values of Γ see, e.g., [10]). It is clear that this model does not predict formation of any stable neutron stars with central baryon number densities below $n_b=0.8$ fm^{-3}. Concerning the calculated speed of sound (the bottom part of Fig. 7), all of the models give v_s/c as being less then 1 up to

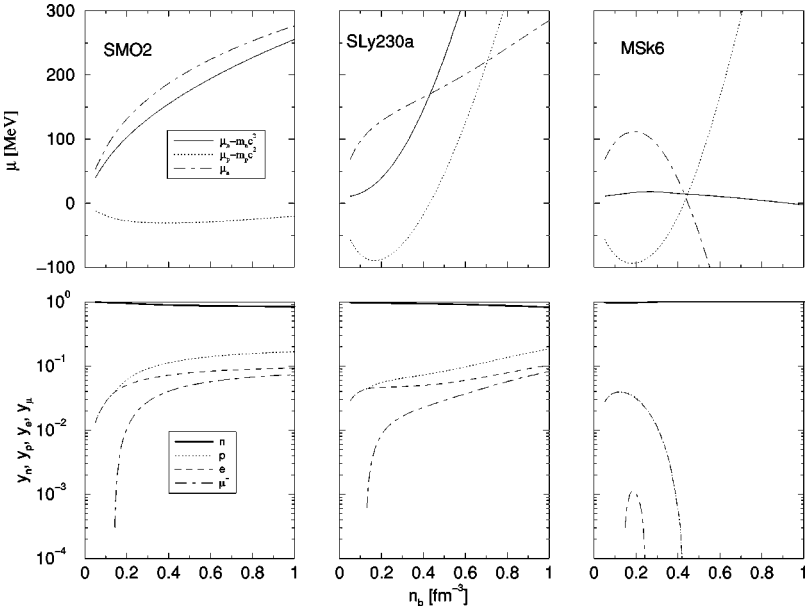

FIG. 6. The neutron, proton, and electron chemical potentials and relative particle fractions for beta-stable matter as calculated with the SMO, SLy230a [6], and MSk6 [31] interactions.

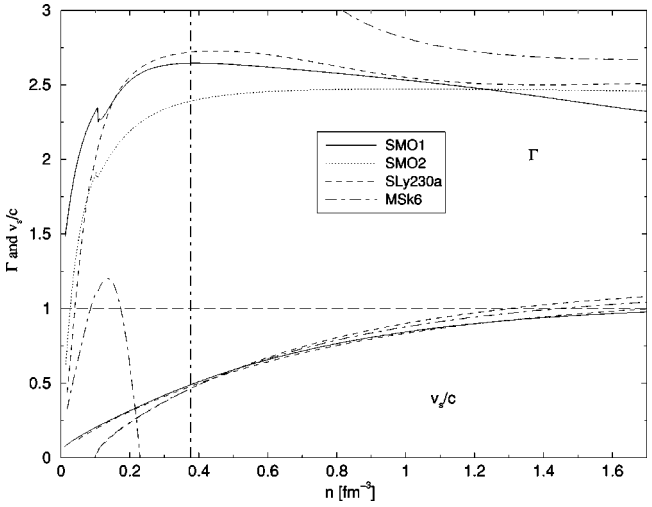

FIG. 7. The adiabatic index Γ and the sound speed as calculated with the SMO1 and SMO2 models. Results for the SLy230a [6] and MSk6 [31] Skyrme models are shown for comparison. See text for explanation.

a density of ~ 1 fm^{-3}, which is well beyond the range of densities where the $n+p+e+\mu$ description is believed to be valid. This is to be expected, as the speed of sound is determined mainly by the incompressibility modulus K, Eq. (8), which is within empirical limits for all of the models considered in Fig. 7.

IV. NEUTRON STARS

A. Properties and observables

A neutron star is an object composed of matter at densities ranging from that of terrestrial iron up to several times that of nuclear matter. For describing this theoretically, it is necessary to use models of atomic and nuclear interactions, from a Fermi gas model for noninteracting particles in the crust of the star, up to ones for hadronic and possibly quark matter in the center of the star. In going from the lowest densities up to $\rho \sim 4.3\times 10^{11}$ g/cm^3 (the neutron drip density [7]), the matter changes from being a nuclear lattice of mainly iron-group nuclei to a system of nuclei that become progressively more neutron rich with the lattice becoming immersed in a free electron gas. Beyond the neutron drip point, free neutrons appear. At densities above $\sim 2\times 10^{14}$ g/cm^3, nuclei no longer exist and the matter consists of nucleon and electron fluids. With further increases of ρ, muons appear and coexist with the neutrons, protons, and electrons in beta equilibrium. At even higher densities, heavier mesons and strange baryons are believed to play a role (see, e.g., [36] and references therein, [8–17,40]). Ultimately, at the center of the star, a quark matter phase may appear, either alone or coexisting with hadronic matter [18–21].

We have constructed an equation of state for zero-temperature beta-stable nucleon+lepton matter using the SMO nucleon-nucleon interaction (both SMO1 and SMO2 parameter sets). Details of the derivation are given in Appendix B. As discussed above, the nucleon+lepton phase forms only a small part of the matter of the star and the SMO EOS needs to be matched, both at lower and higher densities, onto equations of state reflecting the composition of matter at those densities. For lower densities, we used the Baym-Pethick-Sutherland (BPS) EOS [7], matching onto the SMO EOS at ~ 0.1 fm^{-3} and going down to 6.0×10^{-12} fm^{-3}. There are many EOSs available for densities higher than two to three times nuclear saturation density, as mentioned in the Introduction. We chose to use the Bethe-Johnson (BJ) [50] EOS in the density region 0.50–5.02 fm^{-3}, smoothly joining onto the SMO EOS at 0.50 fm^{-3}. The BJ EOS (based on a modified Reid soft core potential and calculated using a constrained variational principle) is now quite old but it has frequently been used as a standard representative one and seems suitable for the present purposes, bearing in mind the continuing uncertainties with ''state of the art'' EOSs for this density range. It treats composite matter consisting of n, p, Λ, $\Sigma^{\pm,0}$, $\Delta^{\pm,0}$, and Δ^{++} in the high density region.

Using a tabulated form of the composite EOSs, we numerically integrated the general relativistic equation of hydrostatic equilibrium for nonrotating stars (the TOV equation [51]),

$$\frac{dP}{dr} = -\frac{Gm\rho}{r^2}\,\frac{(1+P/\rho c^2)(1+4\pi r^3 P/mc^2)}{1-2Gm/rc^2} \qquad (14)$$

with

$$m(r) = \int_0^r 4\pi r^2 \rho(r)\, dr \qquad (15)$$

to obtain sequences of neutron-star models with a range of values for the central density. Integration of Eqs. (14) and (15), for any specified central density, gives directly the corresponding values for the total gravitational mass M and radius R of the star (the surface being at the location where the pressure vanishes).

As mentioned previously, many measured neutron-star masses are close to the canonical value of $1.4M_\odot$ (see [52]) but there are persistent suggestions for some masses being significantly higher than this. The highest mass for which there is solid observational evidence is the $1.44M_\odot$ for the more massive component of the Hulse-Taylor binary pulsar PSR 1913+16 [53]. However, model-based estimates for neutron-star sources showing quasiperiodic oscillations have given some values as high as $1.8M_\odot$ and $2.0M_\odot$ [54,55]. The best case for a neutron star having a mass significantly higher than the canonical value is probably the X-ray pulsar Vela X-1, whose mass has been measured kinematically [56] giving a best value of $1.86M_\odot$ (although the uncertainties are sufficiently great that a mass of around $1.4M_\odot$ cannot be excluded). Observational constraints on the radius are rather uncertain at present (see [57] for a review) but one hopes for improvements in the coming years. Values in the range 10–13 km are generally thought to be reasonable.

We also calculated a number of other key properties of our neutron-star models. The total baryon number is given by

$$A=\int_0^R \frac{4\pi r^2 n(r)dr}{(1-2Gm/rc^2)^{1/2}} \tag{16}$$

and the binding energy released in a supernova core collapse forming the neutron star is approximately $E_{\rm bind}=(Am_0-M)c^2$, where m_0 is the mass per baryon of ^{56}Fe. Analysis of data from supernova 1987A leads to an estimate of $E_{\rm bind}=3.8\pm1.2\times10^{53}$ erg [58]. The gravitational redshift of photons emitted radially outwards from a neutron-star surface is given by

$$z_{\rm surf}=\left(1-\frac{2GM}{Rc^2}\right)^{-1/2}-1. \tag{17}$$

Other quantities of interest for possible comparison with observational data are the minimum rotation period $\tau_{\rm min}$ (see [59]) and the moment of inertia $\mathcal{I}$ (see [60]). The minimum period is given by the centrifugal balance condition for an equatorial fluid element (i.e., the condition for it to be moving on a circular geodesic). While determining this accurately requires using a numerical code for constructing general relativistic models of rapidly rotating stars, quite good values can be obtained from results for nonrotating models using the empirical formula [61,62]

$$\tau_{\rm min}=0.820\left(\frac{M_{\rm max}}{M_\odot}\right)^{-1/2}\left(\frac{R_{\rm max}}{10\ {\rm km}}\right)^{3/2}\ {\rm ms}, \tag{18}$$

where $M_{\rm max}$ and $R_{\rm max}$ are the gravitational mass and radius of the *maximum-mass* nonrotating model for the given EOS. The shortest period so far observed is 1.56 ms [59] but it is possible that this limit may be connected with the techniques used for measuring pulsar periods rather than being a genuine physical limit. The moment of inertia is calculated in a somewhat indirect way. For all pulsars so far observed, the rotation is sufficiently slow that the general relativistic *slow rotation approximation* [63] gives a rather accurate description of the star and the surrounding space-time. Working to first order in the angular velocity Ω of the star, the space-time metric can be written as

$$ds^2=-e^{2\nu}c^2dt^2+e^{2\lambda}dr^2+r^2[d\theta^2+\sin^2\theta(d\phi-\omega dt)^2], \tag{19}$$

where

$$e^{2\lambda}=\frac{1}{1-2Gm/rc^2} \tag{20}$$

and

$$\frac{d\nu}{dr}=\frac{G(m+4\pi Pr^3/c^2)}{r(rc^2-2Gm)} \tag{21}$$

with all quantities referring to the nonrotating reference configuration (before applying the rotational perturbation) apart from ω, which represents the *dragging of the inertial frames* of the space-time in the vicinity of the star. This is the only rotational modification appearing at first order in Ω; rotational deformation of the *shape* of the star and of other components of the metric do not appear until second order. The frame dragging angular velocity ω is calculated from the equation

$$\frac{1}{r^3}\frac{d}{dr}\left(r^4 j\frac{d\omega}{dr}\right)-4\frac{dj}{dr}(\Omega-\omega)=0, \tag{22}$$

where $j=e^{-(\lambda+\nu)}$. In the vacuum outside the star, this has the analytic solution

$$\omega=\frac{2GJ}{c^2r^3}, \tag{23}$$

where J is the angular momentum of the star. It is convenient to work in terms of ω/Ω. By integrating Eq. (22) out from the center and matching both ω and $d\omega/dr$ at the surface with the exterior analytic solution, one can calculate the central value of ω/Ω and the moment of inertia ($\mathcal{I}=J/\Omega$).

B. Results and discussion

Construction of satisfactory neutron-star models requires a detailed knowledge of particle interactions in the nuclear and supernuclear density ranges. As there is still a lot of uncertainty about the details of these interactions, and the available observational data for neutron stars does not yet provide very stringent constraints, all equations of state yielding data within a rather broad range of ''acceptable'' values for relevant observables are viewed as possible descriptions of neutron-star matter. However, while the test for the SMO model provided by neutron-star observations is unfortunately not yet very precise, it is nevertheless valuable to see what predictions this model gives and to compare them with those obtained with other models containing different physics.

We show first in Fig. 8 the calculated gravitational masses of neutron-star models, plotted as a function of radius, obtained for beta-stable nucleon+lepton matter using the SMO1 and SMO2 interactions supplemented by the BPS EOS at low densities and extrapolated up to a density of 1.7 fm^{-3}. Equivalent results for the SLy230a [6] Skyrme interaction and the A18+δv+UIX* potential of Akmal, Pandharipande, and Ravenhall [10] are shown for comparison. It can be seen that all of these EOSs give a maximum mass of around $2M_\odot$ with a similar corresponding radius, but that the values for the radius of a $1.4M_\odot$ ''standard'' star vary significantly (see Tables III and IV). The SMO1 and SMO2 interactions give $R_{1.4}\simeq12.10$ and 11.76 km, respectively, as compared with $R_{1.4}\simeq11.5$ km for the SLy230a and A18 $+\delta v+$UIX* models.

As discussed earlier, the EOS for the beta-stable nucleon +lepton matter is not expected to give a realistic description at densities higher than $(2-3)n_0$, since particles other than neutrons, protons, and leptons are probably present in matter at higher densities. In Fig. 9 we show examples of the relation between gravitational mass and radius for neutron-star

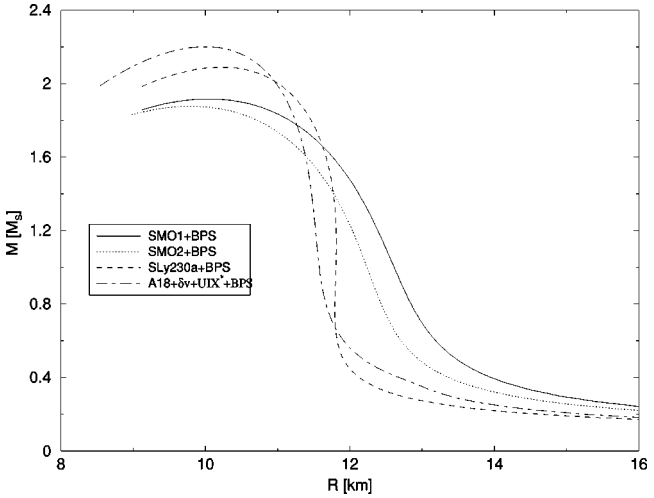

FIG. 8. Gravitational mass plotted against radius for neutron-star models calculated using beta-equilibrium $n+p+\mu+e$ matter extrapolated to higher densities. At low densities, the BPS [7] EOS was used in all cases. For further details and references, see text. Note that here and in the following two figures the unit M_s stands for $M_\odot$.

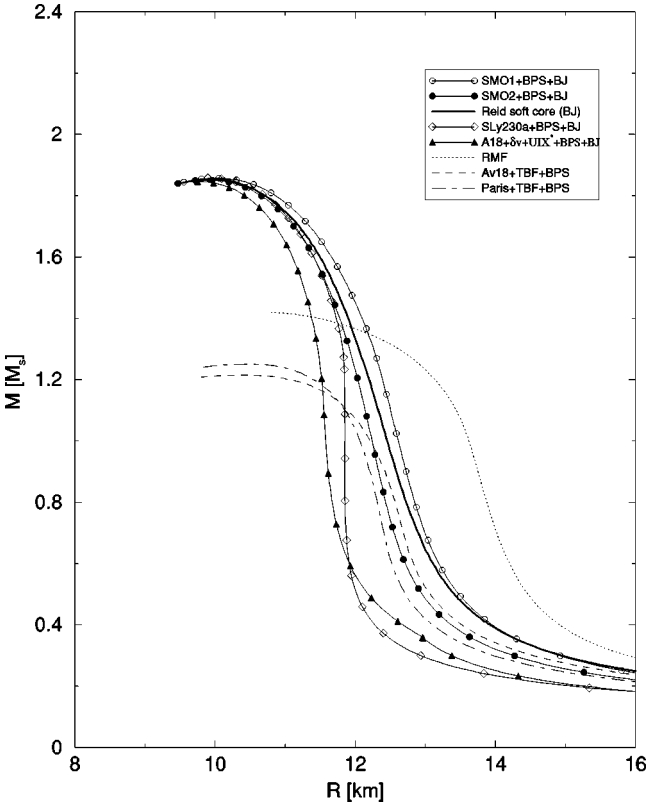

FIG. 9. Gravitational mass plotted against radius for neutron-star models calculated using a high density EOS for hadronic matter containing heavy baryons. All of the EOS's were extended to low densities using the BPS EOS. Results for the SMO1, SMO2, SLy230a, and A18+ δv + UIX* models are compared to predictions from the Bethe-Johnson (BJ) EOS, the RMF EOS [18], and the recent work of Baldo, Burgio, and Schulze [13] based on realistic potentials including three-body forces. For more details see text.

models constructed using EOSs for such multicomponent matter above the threshold for production of heavy baryons. The results given by the SMO1, SMO2, SLy230a, and A18 + δv + UIX* composite EOS's (extended to low densities using BPS and to high densities using BJ in exactly the same way) are compared with those of the original BJ EOS, an RMF EOS of Glendenning (see Table 5.9 in Ref. [18]—this includes the baryon octet together with electrons and muons in generalized beta equilibrium), and two recent calculations using realistic potentials: Av18+ TBF (TBF stands for three-body force) and Paris+ TBF [13]. As expected, the maximum mass calculated with the BJ EOS is essentially the same as those for the composite ones, because the maximum mass is mainly determined by the high density part of the EOS. On the other hand, there are significant differences in the calculated *radii* for lower-mass stars. The composite SMO models show a very similar behavior to that for the original Bethe-Johnson EOS over the whole range of central densities represented here. In contrast, the composite Skyrme-type models (it should be remembered that Akmal, Pandharipande, and Ravenhall [10] use a generalized Skyrme interaction to construct their EOS from the energies of symmetric nuclear matter and pure neutron matter calculated using the A18+ δv + UIX* realistic potential) yield smaller radii and give a steeper decrease in mass, with increasing radius for stars with masses in a region around $1M_\odot$. Although both the SMO and Skyrme interactions are effective models giving very similar saturation properties for infinite symmetric nuclear matter, they are inherently very different. The main point is that their density dependence is not at all the same and so it is not surprising that the corresponding curves for mass against radius should be different in view of the fact that each curve represents a sequence of neutron-star models with a range of central densities. As emphasized by Lattimer and Prakash [57], accurate measurements of the radii of neutron stars could provide a powerful diagnostic for constraining the equation of state at around nuclear matter density, and Fig. 9 shows how such measurements could give a pointer to the relative merits of the SMO and Skyrme pictures.

The maximum mass for the RMF model is just above the expected lower limit $1.44M_\odot$. Surprisingly low maximum masses of $\sim 1.2M_\odot$ have been calculated in the work of Baldo, Burgio, and Schulze [13]; this seems to rule out their model since neutron stars have been observed with masses greater than this and rotation speeds that are not sufficient to raise the maximum mass significantly [53]. Comparison of Figs. 8 and 9 illustrates the softening effect on the EOS caused by the presence of additional types of particles, leading to lower predictions for the maximum mass with multiparticle matter than with nucleon+ lepton matter, as discussed in the preceding section. Hyperon populations in dense matter reduce the energy of the baryon Fermi seas on account of the Pauli principle and consequently reduce the total energy. The baryon pressure, which opposes gravity, is also reduced giving lower maximum masses. Predictions of neutron-star radii, both for maximum-mass models and for $1.4M_\odot$ models differ with different EOS's. Unfortunately,

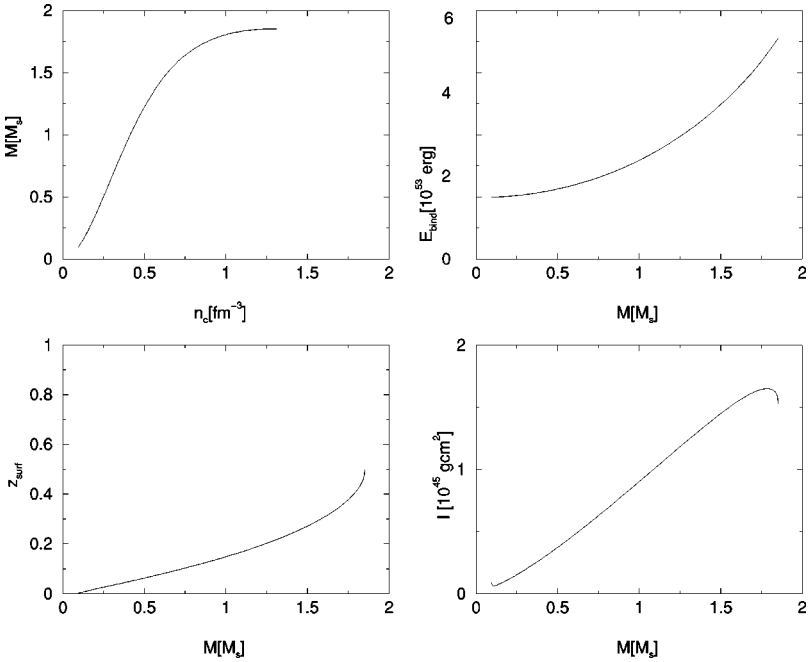

FIG. 10. Results of the neutron-star model calculations for the SMO2+BPS+BJ model. Gravitational mass versus central baryon number density n_c is shown (top left) as well as the binding energy (top right), the gravitational redshift (bottom left), and the moment of inertia (bottom right) plotted versus stellar mass.

however, as mentioned above, the observational limits on radii are rather imprecise and all of the EOS's discussed in this paper give acceptable radii.

In Fig. 10 we show results obtained with the SMO2+BPS+BJ EOS for the gravitational mass plotted as a function of the central baryon number density n_c and the dependence on stellar mass of the binding energy $E_{\rm bind}$, the surface gravitational redshift $z_{\rm surf}$, and the moment of inertia $\mathcal{I}$. For the most part, these do not depend significantly on the high density part of the EOS and the curves are almost identical for the SMO2+BPS and SMO2+BPS+BJ models. Comparison with the results of Chabanat *et al.* [6] for the SLy203a model shows very similar behavior and the results are consistent with expectations for neutron stars.

The numerical results for the neutron-star models calculated using the SMO interactions are summarized in Table III for neutron stars with the maximum mass, and in Table IV for $1.4M_\odot$ models. Again, these are very consistent with expected values and with the results obtained with the SLy230a model. This outcome can be interpreted as a success for the SMO model, which is clearly as adequate for modeling neutron stars as the other models with effective and realistic nucleon-nucleon interactions. Although the present observational constraints on the properties of calculated neutron-star models are not very precise, this situation may well improve greatly in the coming years with advances in observing technology. In particular, gravitational wave data may be extremely useful for constraining neutron-star parameters [65].

V. CONCLUSION

We have here calculated the properties of infinite symmetric and asymmetric nuclear matter using the newly developed separable monopole interactions SMO1 and SMO2. Both interactions give an adequate fit to data for finite nuclei and give excellent agreement with accepted inferred empirical values of nuclear matter observables. For nucleon+lepton matter in beta equilibrium, they predict that the proton fraction y_p would increase with increasing baryon number density, which is in line with present understanding and the predictions of models using a variety of current realistic effective potentials. We have also constructed neutron-star models using a composite EOS, which employs these interactions in the appropriate density range and joins onto other well-established EOS's at lower and higher densities. The different regimes can be made to match well, and the properties of the models calculated in this way are consistent with observational data for real neutron stars. Hence, the separable interaction approach has been shown to work very well both for finite nuclei and for nuclear matter and is now ready for detailed application to a variety of phenomena in nuclear structure.

ACKNOWLEDGMENTS

We thank M. Hjorth-Jensen for supplying the numerical data used in Figs. 4, 5, and 7. This research was sponsored by the Division of Nuclear Physics of the U.S. Department of Energy under Contract No. DE-AC05-00OR 22725 managed by UT-Battelle, LLC and by U.S. DOE Grant No. DE-FG02-94ER40834, the U.K. EPSRC, the Italian Ministero dell'Istruzione, dell'Università e della Ricerca and INFN, and the EU Program ''Improving the Human Research Potential and the Socio-Economic Knowledge Base'' (RTN Contract No. HPRN-CT-2000-00137).

APPENDIX A

We give here a calculation for the observables of symmetric and asymmetric nuclear matter using the separable monopole interaction. We consider general asymmetric nuclear matter characterized by the parameter

$$I=\frac{N-Z}{A}. \tag{A1}$$

The proton and neutron number densities are defined in terms of the I parameter as

$$n_p=\frac{1}{2}(1-I)n, \tag{A2}$$

$$n_n=\frac{1}{2}(1+I)n, \tag{A3}$$

where n is the total number density ($n=n_n+n_p$ in nuclear matter). The kinetic energy per particle for general I is

$$\begin{aligned}\frac{T}{A}&=\frac{\hbar^2}{2m_p}\frac{3}{5}(3\pi^2)^{2/3}\frac{1}{2^{5/3}}(1-I)^{5/3}n^{2/3}\\&\quad+\frac{\hbar^2}{2m_n}\frac{3}{5}(3\pi^2)^{2/3}\frac{1}{2^{5/3}}(1+I)^{5/3}n^{2/3}\\&=c_p\frac{1}{2^{5/3}}(1-I)^{5/3}n^{2/3}+c_n\frac{1}{2^{5/3}}(1+I)^{5/3}n^{2/3},\end{aligned} \tag{A4}$$

where we have introduced two constants c_p and c_n, which will be used later.

We evaluate the potential energy due to our two-body separable interaction in a basis of plane wave states

$$\langle\vec{r}\sigma\tau|\lambda\rangle=\frac{1}{\sqrt{V}}e^{i\vec{k}_\lambda\cdot\vec{r}}\chi_\sigma\xi_\tau. \tag{A5}$$

The total potential energy due to a two-body interaction in a many-body system may be expressed as

$$V=\frac{1}{2}\sum_{\lambda\mu}\left[\langle\lambda\mu|V(1,2)|\lambda\mu\rangle-\langle\lambda\mu|V(1,2)|\mu\lambda\rangle\right]=E_D-E_E, \tag{A6}$$

where λ and μ each represent all of the quantum numbers of the individual particles and the sums run over all occupied states. E_D is referred to as the direct term and E_E as the exchange term. Considering first the direct term, with the isospin-independent part of the two-body interaction acting between the plane wave states, the energy is

$$\begin{aligned}E_D&=\sum_{\xi=a,r}\frac{1}{2}\sum_{k_\lambda\sigma_\lambda\tau_\lambda}^{k<k_F}\sum_{k_\mu\sigma_\mu\tau_\mu}^{k<k_F}\langle k_\lambda\sigma_\lambda\tau_\lambda k_\mu\sigma_\mu\tau_\mu|W_\xi f_{\alpha_\xi}(n)n^{\beta_\xi}n^{\beta_\xi}|k_\lambda\sigma_\lambda\tau_\lambda k_\mu\sigma_\mu\tau_\mu\rangle\\&=\sum_{\xi=a,r}\frac{1}{2}W_\xi\frac{1}{\int n^{\alpha_\xi}d^3r}\left(4\sum_k\frac{1}{V}\int d^3re^{-ik\cdot r}n^{\beta_\xi}e^{ik\cdot r}\right)^2.\end{aligned} \tag{A7}$$

Using the fact that in infinite nuclear matter the density is constant, the quantities n may be taken outside the integrals:

$$E_D=\sum_{\xi=a,r}\frac{1}{2}W_\xi\frac{16}{n^{\alpha_\xi}V}n^{2\beta_\xi}\left(\sum_k^{k_F}1\right)^2=\sum_{\xi=a,r}8W_\xi n^{2\beta_\xi-\alpha_\xi}V^{-1}\left(\tfrac{1}{3}k_F^3V\frac{1}{(2\pi)^3}\right)^2=\sum_{\xi=a,r}A\frac{1}{2}W_\xi n^{2\beta_a-\alpha_\xi+1}, \tag{A8}$$

and so the contribution to the energy, per nucleon, is

$$\frac{E_D}{A}=\frac{1}{2}W_a n^{2\beta_a-\alpha_a+1}+\frac{1}{2}W_r n^{2\beta_r-\alpha_r+1}. \tag{A9}$$

The exchange term E_ξ is given by

$$\begin{aligned}E_\xi&=\sum_{\xi=a,r}\frac{1}{2}\sum_{k_\lambda\sigma_\lambda\tau_\lambda}^{k<k_F}\sum_{k_\mu\sigma_\mu\tau_\mu}^{k<k_F}\langle k_\lambda\sigma_\lambda\tau_\lambda k_\mu\sigma_\mu\tau_\mu|W_\xi f_{\alpha_\xi}(n)n^{\beta_\xi}(\vec{r}_1)n^{\beta_\xi}(\vec{r}_2)|k_\mu\sigma_\mu\tau_\mu k_\lambda\sigma_\lambda\tau_\lambda\rangle\\&=\sum_\xi\frac{1}{2}W_\xi\frac{1}{\int d^3rn}\sum_{k_\lambda\sigma_\lambda\tau_\lambda}^{k<k_F}\sum_{k_\mu\sigma_\mu\tau_\mu}^{k<k_F}\left|\frac{1}{V}\int d^3re^{-ik_\lambda\cdot r}n^\beta e^{ik_\mu\cdot r}\delta_{\sigma_\mu\sigma_\lambda}\delta_{\tau_\mu\tau_\lambda}\right|^2.\end{aligned} \tag{A10}$$

Again taking n to be constant, the integral just gives a δ function:

$$E_\xi=\sum_{\xi=a,r}\frac{1}{2}W_\xi\frac{4}{n^{\alpha_\xi}V}n^{2\beta_\xi}\sum_{k_\lambda}^{k_F}\sum_{k_\mu}^{k_F}\delta_{k_\lambda k_\mu}=\sum_{\xi=a,r}2W_\xi n^{2\beta_\xi-\alpha_\xi}V^{-1}\left(\frac{V}{(2\pi)^3}\int_0^{k_F}4\pi k^2dk\right)=\sum_{\xi=a,r}\frac{1}{2}n^{2\beta_\xi-\alpha_\xi+1} \tag{A11}$$

and the exchange energy per nucleon (E_ξ/A) tends to zero as $A\to\infty$.

When considering asymmetric nuclear matter, there is a contribution to the total energy from the isospin-dependent terms in the interaction. The terms with coefficients a_a and a_r contribute only to the exchange. In this case, the space exchange is the same as the above case (A11) and so no contribution arises from this term in nuclear matter. The direct energy due to the terms with parameters b_a and b_r now depends on the nucleon species. The derivation proceeds as for Eqs. (A7) and (A8), giving

$$E_D = \sum_{\xi=a,r} \frac{1}{2} W_\xi b_\xi n^{2\beta_\xi - \alpha_\xi} V (n_p - n_n)^2, \qquad \text{(A12)}$$

and the energy per particle is

$$E_D/A = \sum_{\xi=a,r} \frac{1}{2} W_\xi b_\xi n^{2\beta_\xi - \alpha_\xi - 1} (n_p - n_n)^2. \qquad \text{(A13)}$$

The energy per particle of general asymmetric nuclear matter can be written in terms of the total density and the asymmetry parameter I using Eqs. (A4), (A9), and (A13):

$$\begin{aligned}\mathcal{E}(n,I) \equiv \mathcal{E}_N &= \frac{T + E_D}{A} \\ &= c_p \frac{1}{2^{5/3}} (1-I)^{5/3} n^{2/3} + c_n \frac{1}{2^{5/3}} (1+I)^{5/3} n^{2/3} \\ &\quad + \frac{1}{2} W_a n^{2\beta_a - \alpha_a + 1} + \frac{1}{2} W_r n^{2\beta_r - \alpha_r + 1} \\ &\quad + \frac{1}{2} W_a b_a n^{2\beta_a - \alpha_a + 1} I^2 + \frac{1}{2} W_r b_r n^{2\beta_r - \alpha_r + 1} I^2. \end{aligned} \qquad \text{(A14)}$$

We label the energy in Eq. (A14) as $\mathcal{E}_N$ for use in the following section (Appendix B) to stress the fact that it represents the nucleon component in beta-stable nucleon+lepton matter.

APPENDIX B

The equation of state of beta-stable nucleon+lepton matter

This matter, consisting of neutrons, protons, electrons, and muons in equilibrium with respect to weak interactions (making the usual assumption that neutrinos leave the system and thus are not contributing to the equilibrium conditions) is characterized by the following processes:

$$n \leftrightarrow p + e^- \leftrightarrow p + \mu^-.$$

Equilibrium implies that the chemical potentials should satisfy the following conditions:

$$\mu_n = \mu_p + \mu_e, \quad \mu_\mu = \mu_e, \qquad \text{(B1)}$$

with each μ being defined by

$$\mu_j = \frac{\partial \epsilon}{\partial n_j}, \qquad \text{(B2)}$$

where ϵ is the total energy density (including the rest masses of the particles involved) and the n_j's are the particle number densities. The latter are used to define particle fractions with respect to the total baryon number density $n_b = n_n + n_p$:

$$y(n_j) = \frac{n_j}{n_b}. \qquad \text{(B3)}$$

The requirement of charge neutrality of the matter implies $n_p = n_e + n_\mu$.

In order to obtain the equation of state, the total energy density of the $n+p+e+\mu$ matter is written as the sum of the nucleon and lepton contributions [6]:

$$\begin{aligned}\epsilon(n_p, n_n, n_e, n_\mu) &= \epsilon_N(n_p, n_n) + n_n m_n c^2 + n_p m_p c^2 + \epsilon_e(n_e) \\ &\quad + \epsilon_\mu(n_\mu) + n_e m_e c^2 + n_\mu m_\mu c^2, \end{aligned} \qquad \text{(B4)}$$

where $\epsilon_N = n_b \mathcal{E}_N$ [see Appendix A, Eq. (A14)]. Given these definitions and conditions, the EOS is determined by two expressions:

$$\rho(n_b) = \frac{\epsilon(n_b)}{c^2}, \quad P(n_b) = n_b^2 \frac{d(\epsilon/n_b)}{dn_b}, \qquad \text{(B5)}$$

where ρ is the mass density of the matter. The EOS is obtained by eliminating n_b between Eqs. (B5) and giving the pressure as a function of the mass density.

The expression for the nucleon energy density can be written, using Eqs. (A14) and (A1)–(A3) and setting $n = n_b$, as

$$\begin{aligned}\epsilon_N(n_b, n_p, n_n) &= c_p n_p^{5/3} + c_n n_n^{5/3} \\ &\quad + \frac{1}{2} W_a n_b^{2\beta_a - \alpha_a + 2} + \frac{1}{2} W_r n_b^{2\beta_r - \alpha_r + 2} \\ &\quad + \frac{1}{2} W_a b_a n_b^{2\beta_a - \alpha_a} (n_n - n_p)^2 \\ &\quad + \frac{1}{2} W_r b_r n_b^{2\beta_r - \alpha_r} (n_n - n_p)^2 \end{aligned} \qquad \text{(B6)}$$

or, in terms of n_b and the baryon fractions (B3), as

$$\begin{aligned}\epsilon_N(n_b, y_p, y_n) &= c_p n_b^{5/3} y_p^{5/3} + c_n n_b^{5/3} y_n^{5/3} + \frac{1}{2} W_a n_b^{2\beta_a - \alpha_a + 2} \\ &\quad + \frac{1}{2} W_r n_b^{2\beta_r - \alpha_r + 2} + \frac{1}{2} W_a b_a n_b^{2\beta_a - \alpha_a + 2} \\ &\quad \times (y_n - y_p)^2 + \frac{1}{2} W_r b_r n_b^{2\beta_r - \alpha_r + 2} (y_n - y_p)^2. \end{aligned} \qquad \text{(B7)}$$

To simplify the calculation, the constants c_p and c_n [defined in Eq. (A4) of Appendix A] are taken to have the same value β, using an average nucleon mass $m = \frac{1}{2}(m_p + m_n)$. The first two terms in Eq. (B7) then become $\beta n_b^{5/3}(y_n^{5/3} + y_p^{5/3})$.

Expression (B7) is then used to calculate the chemical potentials

$$\mu_i = \frac{\partial \epsilon}{\partial n_i} = \frac{\partial(\epsilon/n_b)}{\partial(n_i/n_b)} = \frac{\partial \mathcal{E}}{\partial y_i}, \qquad \text{(B8)}$$

where $\mathcal{E}=\mathcal{E}_N+\mathcal{E}_e+\cdots=\epsilon/n_b$ is the total energy per baryon of the $n+p+e+\mu$ matter. Using expression (B7) and $\mathcal{E}_N=\epsilon_N/n_b$ the proton and neutron chemical potentials are given by

$$\mu_p=\frac{\partial\mathcal{E}_N}{\partial y_p}=\frac{5}{3}\beta n_b^{2/3}y_p^{2/3}-W_a b_a n_b^{2\beta_a-\alpha_a+1}\times(y_n-y_p)-W_r b_r n_b^{2\beta_r-\alpha_r+1}\times(y_n-y_p) \tag{B9}$$

and

$$\mu_n=\frac{\partial\mathcal{E}_N}{\partial y_n}=\frac{5}{3}\beta n_b^{2/3}y_n^{2/3}+W_a b_a n_b^{2\beta_a-\alpha_a+1}\times(y_n-y_p)+W_r b_r n_b^{2\beta_r-\alpha_r+1}\times(y_n-y_p). \tag{B10}$$

The expressions for the lepton chemical potentials can be obtained using expression (B8) and the energy densities (calculated with the Fermi-gas model for noninteracting fermions [64]),

$$\epsilon_e\approx\frac{1}{4\pi^2}\frac{\mu_e^4}{(\hbar c)^3} \tag{B11}$$

$$\epsilon_\mu=\frac{1}{4\pi^2(\hbar c)^3}\left[\mu_\mu k\left(\mu_\mu^2-\frac{1}{2}m_\mu^2c^4\right)-\frac{1}{2}m_\mu^4c^8\ln\left(\frac{\mu_\mu+k}{m_\mu c^2}\right)\right], \tag{B12}$$

where $k=(3\pi^2y_\mu n_b)^{1/3}\hbar c$. The electron energy is that for the ultrarelativistic limit. Also, there is a contribution from the Coulomb interaction. The direct term is zero due to the charge neutrality of the system, but the exchange term provides a small contribution [4]:

$$\epsilon_{\rm ce}=-\frac{3}{2}\left(\frac{3}{\pi}\right)^{1/3}e^2(y_e n_b)^{4/3}. \tag{B13}$$

It follows that

$$\mu_e=\hbar c(3\pi^2y_e n_b)^{1/3} \tag{B14}$$

and

$$\mu_\mu=\sqrt{(m_\mu c^2)^2+\hbar^2c^2(3\pi^2y_\mu n_b)^{2/3}}. \tag{B15}$$

Below the threshold for the creation of μ^-, the equilibrium condition holds:

$$\mu_n-\mu_p-\mu_e=0. \tag{B16}$$

Charge neutrality of the matter implies that $y_p=y_e$; since $y_p+y_n=1$, condition (B16) can be rewritten as a function of y_p only and solved for the equilibrium value of y_p at a given density n_b.

Above the muon threshold (i.e., when the difference between the neutron and proton chemical potentials exceeds the rest mass of the muon) we have

$$\mu_n-\mu_p=\mu_\mu,\quad \mu_\mu=\mu_e, \tag{B17}$$

together with the charge neutrality requirement,

$$y_p=y_e+y_\mu\quad\text{giving}\quad y_n=1-y_p=1-y_e-y_\mu. \tag{B18}$$

The equilibrium electron fraction and muon fraction can be related via Eqs. (B14) and (B15):

$$y_e=\left[\left(\frac{m_\mu c^2}{\hbar c}\right)^2\frac{1}{(3\pi^2n_b)^{2/3}}+y_\mu^{2/3}\right]^{3/2}, \tag{B19}$$

and by combining Eqs. (B17)–(B19), the equilibrium relative fractions y_p, y_e, and y_μ can be calculated for any given baryon number density n_b.

Now that the entire expression for the energy density is known, the pressure can be evaluated. Since the protons and neutrons interact strongly, their separate partial pressures cannot be defined. Instead, the nucleon pressure is calculated:

$$\begin{aligned}P_N&=n_b^2\frac{\partial(\epsilon_N/n_b)}{\partial n_b}\\&=n_b^2\frac{\partial\mathcal{E}_N}{\partial n_b}\\&=\frac{2}{3}\beta n_b^{5/3}(y_n^{5/3}+y_p^{5/3})\\&\quad+\frac{1}{2}(2\beta_a-\alpha_a+1)W_a n_b^{2\beta_a-\alpha_a+2}\\&\quad+\frac{1}{2}(2\beta_r-\alpha_r+1)W_r n_b^{2\beta_r-\alpha_r+2}\\&\quad+\frac{1}{2}(2\beta_a-\alpha_a)W_a b_a n_b^{2\beta_a-\alpha_a+2}(y_n-y_p)^2\\&\quad+\frac{1}{2}(2\beta_r-\alpha_r)W_r b_r n_b^{2\beta_r-\alpha_r+2}(y_n-y_p)^2.\end{aligned} \tag{B20}$$

The electron and muon pressures and the Coulomb exchange pressure are calculated in the same way to be

$$P_e=\frac{1}{12\pi^2}\frac{\mu_e^4}{(\hbar c)^3}, \tag{B21}$$

$$P_\mu=\frac{1}{12\pi^2}\frac{1}{(\hbar c)^5}\left[\mu_\mu k\left(\mu_\mu^2-\frac{5}{2}m_\mu^2c^4\right)+\frac{3}{2}m_\mu^4c^3\ln\left(\frac{\mu_\mu+k}{m_\mu c^2}\right)\right], \tag{B22}$$

$$P_{\rm ce}=-\frac{1}{2}\left(\frac{3}{\pi}\right)^{1/3}e^2(y_e n_b)^{4/3}, \tag{B23}$$

where the momentum in the expression for the muon pressure is $k=(3\pi^2y_\mu n_b)^{1/3}\hbar c$.

[1] D. Vautherin and D. M. Brink, Phys. Rev. C **3**, 626 (1972).
[2] J. Decharge and D. Gogny, Phys. Rev. C **21**, 1568 (1980).
[3] J. M. Lattimer, C. J. Pethick, D. G. Ravenhall, and D. Q. Lamb, Nucl. Phys. **A432**, 646 (1985).
[4] M. Onsi, H. Przysiezniak, and J. M. Pearson, Phys. Rev. C **50**, 460 (1994).
[5] C. J. Pethick, D. G. Ravenhall, and C. P. Lorenz, Nucl. Phys. **A585**, 675 (1995).
[6] E. Chabanat, P. Bonche, P. Haensel, J. Meyer, and R. Schaeffer, Nucl. Phys. **A627**, 710 (1997).
[7] G. Baym, C. Pethick, and P. Sutherland, Astrophys. J. **170**, 299 (1971).
[8] R. B. Wiringa, V. Fiks, and A. Fabrocini, Phys. Rev. C **38**, 1010 (1988).
[9] R. B. Wiringa, Rev. Mod. Phys. **65**, 231 (1993).
[10] A. Akmal, V. R. Pandharipande, and D. G. Ravenhall, Phys. Rev. C **58**, 1804 (1998).
[11] H. Heiselberg and M. Hjorth-Jensen, Phys. Rep. **328**, 237 (2000).
[12] S. Balberg and A. Gal, Nucl. Phys. **A625**, 435 (1997).
[13] M. Baldo, G. F. Burgio, and H.-J. Schulze, Phys. Rev. C **61**, 055801 (2000).
[14] I. Vidana, A. Polls, A. Ramos, L. Engvik, and M. Hjorth-Jensen, Phys. Rev. C **62**, 055801 (2000).
[15] J. Schaffner and I. N. Mishustin, Phys. Rev. C **53**, 1416 (1996).
[16] F. de Jong and H. Lenske, Phys. Rev. C **57**, 3099 (1998).
[17] C. M. Keil, F. Hoffmann, and H. Lenske, Phys. Rev. C **61**, 064309 (2000).
[18] N. K. Glendenning, *Compact Stars*, 2nd ed. (Springer, New York, 2000), Chaps. 8 and 9.
[19] S. Pal, M. Hanauske, I. Zakout, H. Stocker, and W. Greiner, Phys. Rev. C **60**, 015802 (1999).
[20] K. Schertler, S. Leupold, and J. Schaffner-Bielich, Phys. Rev. C **60**, 025801 (1999).
[21] M. Hanauske, D. Zschiesche, S. Pal, D. Schramm, H. Stocker, and W. Greiner, Astrophys. J. **537**, 50320 (2000).
[22] P. Stevenson, M. R. Strayer, and J. Rikovska-Stone, Phys. Rev. C **63**, 054309 (2001).
[23] C. Mahaux and R. Sartor, in *Nuclear Matter and Heavy Ion Collisions*, Vol. 205 of NATO Advanced Studies Institute, Series B: Physics, edited by M. Soyeur (Plenum, New York, 1989), Vol. 205, p. 1.
[24] J. R. Nix and P. Moller, in *Invited Paper at the International Conference on Exotic Nuclei and Atomic Masses, Arles, France*, 1995, edited by M. de Saint Simon and D. Sorlin (Editions Frontieres, Gif-sur-Yvette, 1995), p. 23
[25] J. P. Blaizot, Phys. Rep. **64**, 171 (1980).
[26] P. Gleissl, M. Brack, J. Meyer, and P. Quentin, Ann. Phys. (N.Y.) **197**, 205 (1990).
[27] J. P. Blaizot, J. F. Berger, J. Decharge, and M. Girod, Nucl. Phys. **A591**, 435 (1995).
[28] M. Farine, J. M. Pearson, and F. Tondeur, Nucl. Phys. **A615**, 135 (1997).
[29] C. F. Von Weizsäcker, Z. Phys. **96**, 431 (1935).
[30] P. Moller, W. D. Meyers, W. J. Swiatecki, and J. Treiner, At. Data Nucl. Data Tables **59**, 225 (1995).
[31] F. Tondeur, S. Goriely, J. M. Pearson, and M. Onsi, Phys. Rev. C **62**, 024308 (2000).
[32] Bao-An Li, C. M. Ko, and Z. Ren, Phys. Rev. Lett. **78**, 1644 (1997).
[33] X. Vinas, M. Barranco, J. Treiner, and S. Stringari, Astron. Astrophys. **182**, L34 (1987).
[34] P.-G. Reinhard, D. J. Dean, W. Nazarewicz, J. Dobaczewski, J. A. Maruhn, and M. R. Strayer, Phys. Rev. C **60**, 014316 (1999).
[35] B. A. Brown, Phys. Rev. C **58**, 220 (1998).
[36] W. D. Arnett and R. L. Bowers, Astrophys. J., Suppl. **33**, 415 (1977).
[37] B. Arntsen and E. Ostgaard, Phys. Rev. C **30**, 335 (1984).
[38] G. Bao, L. Engvik, M. Hjorth-Jensen, E. Osnes, and E. Ostgaard, Nucl. Phys. **A575**, 707 (1994).
[39] S. Balberg, I. Lichtenstadt, and G. B. Cook, Astrophys. J., Suppl. **121**, 515 (1999).
[40] V. R. Pandharipande, Nucl. Phys. **A178**, 123 (1971).
[41] Th. A. Rijken, Nucl. Phys. **A639**, 29c (1998).
[42] B. F. Gibson and E. V. Hungerford, Phys. Rep. **257**, 349 (1995).
[43] J. J. de Swart, P. M. M. Maessen, and Th. A. Rijken, in *Properties and Interactions of Hyperons*, edited by B. F. Gibson *et al.* (World Scientific, Singapore, 1994), p. 37.
[44] C. J. Pethick, Rev. Mod. Phys. **64**, 1133 (1992).
[45] M. Prakash, Phys. Rep. **242**, 191 (1994).
[46] M. Colpi, U. Geppert, D. Page, and A. Possenti, Astrophys. J. Lett. **548**, L175 (2001).
[47] T. Suzuki, H. Geissel, O. Bochkarev, L. Chulkov, M. Golovkov, N. Fukunishi, D. Hirata, H. Irnich, Z. Janas, H. Keller, T. Kobayashi, G. Kraus, G. Munzenberg, S. Neumaier, F. Nickel, A. Ozawa, A. Piechaczeck, E. Roeckl, W. Schwab, K. Summerer, K. Yoshida, and I. Tanihata, Nucl. Phys. **A630**, 402c (1998).
[48] N. K. Glendenning, Astrophys. J. **293**, 470 (1985).
[49] J. Mares, E. Friedman, A. Gal, and B. K. Jennings, Nucl. Phys. **A594**, 311 (1995).
[50] H. A. Bethe and M. Johnson, Nucl. Phys. **A230**, 1 (1974).
[51] R. C. Tolman, Proc. Natl. Acad. Sci. U.S.A. **20**, 3 (1934); J. R. Oppenheimer and G. M. Volkov, Phys. Rev. **55**, 374 (1939).
[52] S. Thorsett and D. Chakrabarty, Astrophys. J. **512**, 288 (1999).
[53] J. H. Taylor and J. M. Weisberg, Astrophys. J. **345**, 434 (1989).
[54] M. C. Miller, F. K. Lamb, and D. Psaltis, Astrophys. J. **508**, 791 (1998).
[55] L. Stella and M. Vietri, Astrophys. J. Lett. **492**, L59 (1998).
[56] O. Barziv, L. Kaper, M. H. van Kerkwijk, J. H. Telting, and J. van Paradijs, Astron. Astrophys. **377**, 925 (2001).
[57] J. M. Lattimer and M. Prakash, Astrophys. J. **550**, 426 (2001).
[58] R. Schaffer, Y. Declais, and S. Julian, Nature (London) **300**, 142 (1987).
[59] N. K. Glendenning, *Compact Stars* (Ref. [18]), p. 213.
[60] S. L. Shapiro and S. A. Teukolsky, *Black Holes, White Dwarfs and Neutron Stars* (Wiley, New York, 1983), Chap. 10.
[61] P. Haensel and J. L. Zdunik, Nature (London) **340**, 617 (1989).
[62] P. Haensel, M. Salgado, and S. Bonazzola, Astron. Astrophys. **296**, 745 (1994).
[63] J. B. Hartle, Astrophys. J. **150**, 1005 (1967).
[64] N. K. Glendenning, *Compact Stars* (Ref. [18]), Chap. 3.
[65] V. Ferrari, J. C. Miller, and L. Rezzolla, *Gravitational Waves: A Challenge to Theoretical Astrophysics*, ICTP Lecture Series Vol. 3 (ICTP, Trieste, 2001).